Desalination and Water Treatment
www.deswater.com

doi:10.5004/dwt.2018.22738

132 (2018) 157–166
November

Photocatalytic performance of SiO_2-TiO_2 composite via F-assisted restructure of Ti-bearing slag

Jizhi Zhou, Hao Hou, Mao Lin, Yongwen Su, Yongsheng Lu, Jia Zhang*, Guangren Qian

School of Environmental and Chemical Engineering, Shanghai University, No.99 Shangda Rd., Shanghai 200444, China, email: jizhi.zhou@t.shu.edu.cn (J. Zhou), majestic@i.shu.edu.cn (H. Hou), lm0813@yeah.net (M. Lin), 965957410@qq.com (Y. Su), Tel. +862166137746. Fax +86 21 66137761, email: irujam@t.shu.edu.cn (J. Zhang), email: 273918409@qq.com (G. Qian)

Received 2 November 2017; Accepted 4 July 2018

ABSTRACT

In this work, the formation of SiO_2 coated TiO_2 (SiO_2-TiO_2) composite from titanium bearing blast furnace slag (TBBFS) was carried out by hydrothermal treatment in the acidic solution with the assistance of F^-. The basanite and perovskite were two main compositions in TBBFS which provided Si and Ti for the SiO_2-TiO_2 composite formation, respectively. For this purpose, the HCl solution was used as leaching agent in the hydrothermal treatment of TBBFS at 180°C, which led to Si and Ti leaching for the formations of anatase TiO_2 phase and amorphous SiO_2 phase. In comparison, the leaching process in HF led to the formation of metal fluorides and TiO_2 with the dissolution of most Si. Accordingly, different amount of HF addition in HCl leaching of TBBFS led to the SiO_2/TiO_2 mass ratio in composite varying from 1.1 to 3.7. Moreover, the various mass ratio of SiO_2 to TiO_2 in the composite resulted in the different photodegradation performance of Rhodamine B, where 95% of Rhodamine B was removed on the composite at 1.1–1.2 of SiO_2/TiO_2 mass ratio. The adsorption of positive dye on negative SiO_2 and the simultaneous photodegradation on available TiO_2 surface were responsible for the effective Rhodamine B removal. Therefore, our result provided a facile approach to the preparation of photocatalyst candidate from TBBFS for the degradation of organic contaminate in the solution.

Keywords: Titanium bearing blast furnace slag; Hydrothermal treatment; Anatase; Photocatalyst

1. Introduction

The catalytic degradation of organic contaminates was the common technology in water treatment [1–3]. There have been many methods developed to achieve the water purification [4]. Among these methods, TiO_2 photocatalytic technology has been attracted much attention as it is the most efficient, environmentally benign and promising method to remove contaminate [5,6]. To improve the photocatalytic activity and photodegradation performance of TiO_2, the TiO_2 surface was coated by Al_2O_3 [7], SiOx [8], MgOx [9] particles. Among these development of TiO_2 photocatalyst, amorphous silica, MCM-41 [10] and SBA-15 [11] was often coated on TiO_2. As the negative surface of SiO_2, the coating of SiO_2 on TiO_2 enhanced the adsorption of positive contaminates such as Rhodamine B [12–14], which led to the increase of its photodegradation kinetics on the composite. The other advantage of SiO_2 coating was to separate the photogenerated electrons and holes in TiO_2, which resulted in the improvement of photocatalytic activity for removal of organic compounds [15–18]. Many strategies for preparing the SiO_2 coated TiO_2 were proposed [19–21]. However, in these methods, the laboratory reagents were always used as Si and Ti sources, which cost was high. Thus, an approach to the low-cost preparation of the composite is necessary.

Titanium bearing blast furnace slag (TBBFS), from iron and steel industry, usually contains 10–20% of Ti, 20–30% of Si, 10% of Al, and other metals. In the recovery of TBBFS, TiO_2 is the common product [22,23]. However, only 50%–60% of Ti was extracted for TiO_2 formation in practical industrial process. The residue after the Ti recovery was

*Corresponding author.

treated as the additional material in cement, concrete production or roadbed [24,25]. In China, there are more than three million tons of titanium-bearing blast furnace slag industry each year [26,27]. The low recovery efficiency of Ti leads to the challenge to the loss of Ti in TBBFS for resource recovery. Therefore, a new strategy is proposed to recover the elements except Ti in the high-value way of utilization. Based on the development of SiO_2-TiO_2 catalyst, it is expected that the SiO_2 coated anatase TiO_2 can be prepared from TBBFS to achieve the recovery of both Ti and Si.

In TBBFS, perovskite ($CaTiO_3$) is the predominant Ti species, which was converted to TiO_2 through the acid leaching, high-energy ball milling, alkaline-thermal treatment, catalytic applications [28–31]. Among these processes, the hydrothermal treatment with acidic solution was an important method to prepare TiO_2 with high activity [28]. On the other hand, the formation of SiO_2 particles was also achieved by hydrothermal treatment from Si-waste [32]. Accordingly, the formation of SiO_2 coated TiO_2 composite from TBBFS is suggested through hydrothermal treatment in acidic solution.

In this work, we aim to develop an approach to the preparation of amorphous SiO_2 coated anatase TiO_2 from TBBFS. The hydrothermal treatment of TBBFS in HCl and HF solution was performed. After treatment, the composition in the residue was characterized. Based on these result, the mixture with HCl and HF at various [HF]s was used to prepare the SiO_2 coated TiO_2 photocatalyst. Its photocatalysis performance was conducted in the photo-reduction of Rhodamine B under UV irradiation.

2. Experimental section

2.1. Leaching of TBBFS

TBBFS was provided by Panzhihua Iron and Steel Corporation of China. The composition of TBBFS is shown in Table 1. The TBBFS was ground in a high-energy ball mill prior to the treatment.

The leaching of TBBFS was carried out by hydrothermal treatment. Typically, 0.5 g of TBBFS powder was added in 40 mL of 1 mol/L HCl. The mixture was then transferred into a 50 mL teflon lined stainless steel autoclave. The sealed autoclave was heated at 180°C in an oven for 1–10 h. After cooling in the atmosphere, the suspension was taken out from the autoclave. The solid precipitate was separated by centrifugation, washed by distilled water and dried overnight in an oven. The liquid was collected for further determination.

Table 1
The composition of TBBFS (%, w/w)

Sample	TBBFS
Si	11.9
Ti	11.8
Ca	19.2
Al	6.29
Mg	6.98
Fe	1.83

In similar way, the HF-assisted leaching of TBBFS was performed with 0.4–1.0 mol/L of HF added in the HCl leach solution above. Accordingly, the as-prepared composite was denoted as HF1.0, HF0.8, HF0.6 and HF0.4, respectively.

2.2. Photocatalytic activity evaluation

The photocatalysis of the composite was evaluated by the photodegradation of Rhodamine B (RB) under UV irradiation. Briefly, 0.040 g of the composite was added in 40 mL of RB solution with the RB concentration of 25 mg/L. The photocatalysis of this suspension was performed in a double wall jacket quartz photoreactor (Bi Lon, China) of cylindrical shape at 25 ± 1°C. A 125 W medium pressure Hg lamp (GGZ, Jiguan, China) emitted predominantly at 365–366 nm was immersed within the photoreactors as UV irradiation source. With continuously magnetic stirring, the photo-reaction was carried out for 60 min. For the kinetics of the photocatalysis, the reaction above was repeated at various time. After reaction, the suspension was separated by centrifuge. The solid sample was washed by distilled water and dried overnight in an oven. The aqueous solution was collected for further determination. In the similar way, the adsorption of RB on the composite was carried out without UV irradiation.

2.3. Characterization

The X-ray diffraction of the solid sample was carried out on a D/MAX-2200 X-ray diffractometer (Rigaku, Japan) using Cu Kα radiation (λ = 0.15406 nm) at 40 kV, at a scanning rate of 2° min^{-1}. Powder data file (ICDD-JCPDS) was utilized for analysis of the patterns. The surface area of the samples was measured by N_2 sorption at liquid nitrogen temperature in a Quantasorb SI Analyser (Quantachrome Co., USA). The morphology of the solid sample powders were recorded by a scanning electron microscopy S-3000N (HITACHI, Japan) equipped with an energy dispersive X-ray spectroscopy (EDXs) analysis unit.

The composition of TBBFS was measured by X-ray Fluorescence Spectrometer (XRF-1800, SHIMADZU LIMITED, Japan). The WFZ UV-4802H (UNICO, China) spectrophotometer was employed to determine the concentration of Si and Rhodamine B in the treated solution by following the corresponding methods [33]. Before the Si determination, 1 ml of HF (0.02 mol/L) was added in the solution to ensure the Si dissolution. The concentration of metal in the solution was determined by Inductively Coupled Plasma-Atom Emission Spectrum (ICP-AES, Prodigy, Leeman Co.).

3. Results and discussion

3.1. Characterization of SiO_2-TiO_2 composite in TBBFS leaching

Table 1 lists the composition of TBBFS, indicating that Ca, Ti, Si were the main elements in TBBFS. The XRD pattern of raw TBBFS is illustrated in Fig. 1, where sharp peaks of basanite (PDF = 88-0847) and perovskite (PDF = 77-0182) were identified raw TBBFS. Accordingly, it is proposed that in the raw TBBFS, Ti was predominant in perovskite phase with near 50% (w/w) of Ca while Si in basanite with

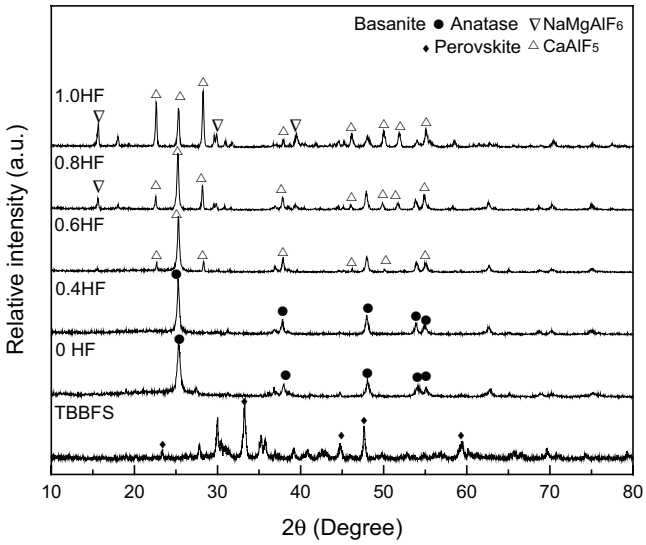

Fig. 1. X-ray diffraction patterns of leaching slag with 1 mol/L HCl and x mol/L HF (x = 0, 0.4, 0.6, 0.8, 1), S/L = 0.5 g/40 ml, time = 7 h, compared with that of pristine slag.

Ca, Mg, Al, Fe. Moreover, Fig. 1 shows the XRD patterns of the collected solid after hydrothermal treatment at 180°C in HCl solution with various dosages of HF addition. In the case of HCl leaching (HF0), no perovskite and basanite phases were identified by XRD, indicating the collapse of the TBBFS in hydrothermal treatment. Instead, a series of diffraction peaks at 25.3°, 38.0°, 48.1°, 54.1°, and 55.1° (2θ) was recorded in the XRD pattern of HF0, which was indexed as anatase phase (PDF = 86-1157). This demonstrates the complete conversion of perovskite to TiO_2 in the HCl solution, consistent with the result elsewhere [27]. Besides, a small portion of rutile phase was formed as the peak at 27.2° of rutile-TiO_2 in HF0. In comparison, there was no Si bearing phase appeared in HF0. This observation suggests that the amorphous SiO_2 was probably the fate of basanite conversion.

The TiO_2/SiO_2 composite was often prepared by the hydrolysis of Ti and Si precursor. In this way, TiO_2 was formed as its faster deposition than that of SiO_2. Accordingly, Si always adsorbed on the TiO_2 surface, resulting in the formation of SiO_2-covered TiO_2 composite [34,35]. In our case, the HCl leaching treatment of slag was supposed to lead to the formation of TiO_2/SiO_2 composite as the hydrolysis of slag, consistent with that in the previous report [36].

With the HF addition, the strong diffraction peaks of anatase phase instead of the perovskite and basanite were also identified in the XRD pattern of all cases with HF added (HF0.4–HF1.0). This demonstrates the similar conversion process of TBBFS to that in HF0. The rutile phase was disappeared with HF addition, indicating that F^- improves the formation of anatase phase. However, with the increase in the HF concentration to 1.0 mol/L, the new reflections of $NaMgAlF_5$ and $CaAlF_5$ were recorded in the solid samples, which resulted in metal fluoride impurity in the leaching product. As basanite was composed of Na, Mg, Si in the raw slag, the formation of $NaMgAlF_5$ after acid leaching suggests Na was leached out and reprecipitated in the new

Table 2
Leaching percentage of compositions in TBBFS after hydrothermal treatment at 180°C in 1 mol/L HCl solution with various HF addition

Treatment	Si[a]	Ti[b]	Ca[b]	Al[b]	Mg[b]	Fe[b]
0.4HF	19.2	11.0	91.9	78.5	96.7	97.9
0.6HF	31.8	21.9	90.1	70.5	86.2	98.2
0.8HF	33.5	73.7	72.2	66.4	86.2	98.3
1.0HF	41.8	55.7	51.6	51.9	79.5	98.1

[a]was determined by ultraviolet spectrophotometry
[b]were determined by ICP analysis

phase with F. Therefore, it is proposed that the low [HF] did not impact on the product in HCl leaching.

The leaching percentage of main elements in TBBFS after treatment was listed in Table 2, with the balance of these elements in the solution and solid (Table S1). With [HF] increasing to 1.0 mol/L, the leaching percentage of Si was increased to 41.8%. In comparison, the leaching percentage of Ti was 73.7% at [HF] of 0.8 mol/L and 55.7% at [HF] of 1.0 mol/L, much higher than that in the case of lower [HF]. This suggests that [HF] at 0.8 mol/L or more removed large amount of Ti from TBBFS, which reduced the amount of TiO_2 formed. Accordingly, the mass ratio of SiO_2 to TiO_2 in the composite was 1.1–1.2 at [HF] < 0.6 mmol/L while increased to 1.7–3.3 at [HF] > 0.8 mmol/L. Besides, Ca, Al, Mg and Fe were also dissolved in the acidic solution. With [HF] < 0.8 mol/L, the leaching percentage of Ca and Al was about 90–92% and 70–78% respectively, higher than that in the case of [HF] > 0.8 mol/L. This indicates most of Ca and Al were removed from TBBFS at low [HF].

Fig. 2A shows the aggregates of the particle in the solid product after HCl leaching without HF. The EDX-mapping reflection of Si (Fig. 2A1) and Ti (Fig. 2A2) was overlapped, indicating that the TiO_2 substrate was almost covered by SiO_2. This suggests that the product after acidic leaching was the composite of TiO_2 and SiO_2. However, the photocatalytic efficiency of the SiO_2-TiO_2 composite in this case was probably reduced as the poor light penetration of SiO_2. Fig. 2B illustrates the SEM image and EDX mapping result of TBBFS after treatment with 0.6 mol/L of HF as example. Compared to that without HF, the reflection of Si was collected on partial surface of TiO_2 in the composite after leaching treatment with HF addition, despite the similar morphology in both cases. Taking into account the tunable SiO_2/TiO_2 mass ratio by HF addition, the EDX mapping result demonstrates that the addition of HF in HCl hydrothermal treatment of TBBFS can improve the exposure of TiO_2 surface. In consequence, it is suggested that the high photocatalysis performance of the composite is probably achieved by the decrease in the coverage of SiO_2 on TiO_2 surface.

On the other hand, the reduction of SiO_2 may lead to the decreasing of specific surface area (SSA) on the composite. As shown in Fig. S1, the N_2 adsorption-desorption curve of HF0.6 exhibited smaller specific surface area (SSA) than that of the sample after treatment without HF. This means that the adsorption capacity of HF0.6 is probably weaker than that of HF0. Despite, the loading of SiO_2 on

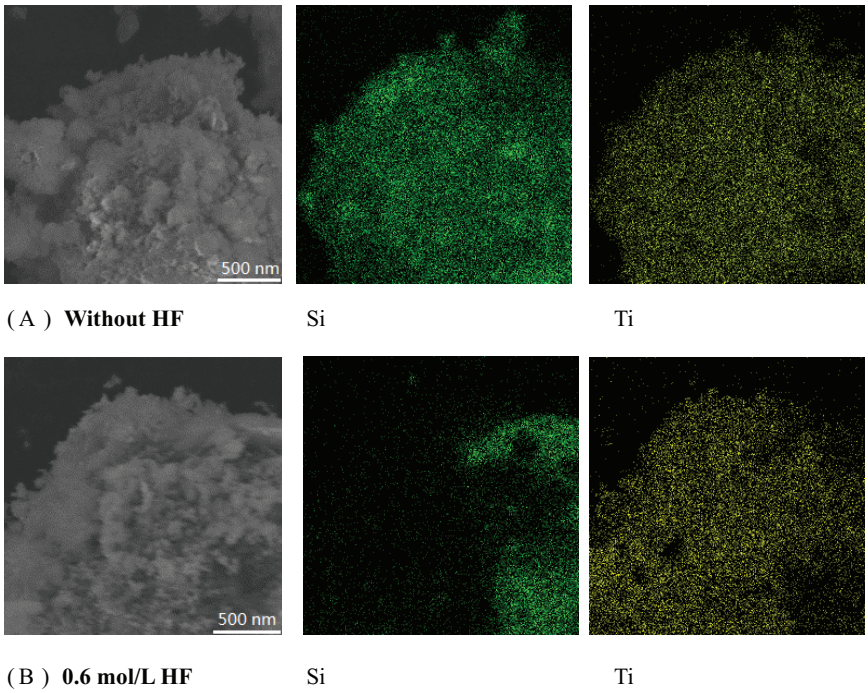

Fig. 2. SEM image of the solid after hydrothermal treatment in HCl solution without HF (A) and with 0.6 mol/L of HF (B), and the corresponding EDX elemental mapping of Si and Ti.

the composite probably still increases the negative charge on TiO_2 surface, which probably enhances the adsorption of positive contaminate on the TiO_2 for photodegradation [37]. Therefore, it is proposed that the HF treatment can improve the photocatalysis performance of the composite as more TiO_2 surface exposure combined with the adsorption of contaminate on SiO_2.

3.2. Effect of time on TBBFS conversion

In the TBBFS leaching, the time plays an important role in the formation of TiO_2. Fig. 3A illustrates the evolution of TBBFS phase after leaching for various time in HCl leach solution. The anatase and perovskite phases were identified in XRD pattern of the solid sample after 2 h leaching. With the increase in leaching time, the diffraction peak of perovskite phase became weak in 4 h and vanished in 10 h. This demonstrates that the complete conversion of perovskite to TiO_2 should take over 4 h. Despite, the leaching for long time led to the conversion of anatase phase due to the diffraction reflection of rutile phase in the sample after 10 h treatment. As the lower photocatalytic activity of rutile than that of anatase, the leaching process should be carried out less than 10 h.

Fig. 3B shows the XRD patterns of TBBFS after HF-assisted leaching process for various time. With 0.6 mol/L of HF, the anatase phase with basanite and perovskite phase was identified in the solid sample after 1 h treatment. As the increase in the leaching time, the basanite and perovskite phases were disappeared. There were anatase phase with a portion of $CaAlF_5$ observed in the leached sample for 2–10 h. This indicates that the assistance of HF in the HCl leaching process promoted the conversion of TBBFS to SiO_2-TiO_2 composite. It is noting that no rutile phase was recorded in long time leaching process, even for 10 h. This inhibition of rutile phase is contributed to the improvement of dominated {001} facet of TiO_2 by F^- [38,39]. Therefore, it is suggested that the SiO_2-TiO_2 composite can be prepared from TBBFS leaching in 2 h with the assistance of HF.

3.3. Effect of temperature on the composite formation

Fig. 4A shows the XRD pattern of the solid sample after hydrothermal treatment in HCl solution at various temperatures. At 100 and 150°C, the diffraction peaks of basanite and perovskite were still recorded without that of TiO_2. This retaining of TBBFS contents indicates that Ti and Si was not leached out at low leaching temperature as the disappearing of perovskite and basanite phases in the collected solid after treatment at 180°C. Fig. 4B illustrates the XRD reflections of basanite and perovskite in the treated sample with HF at 100 and 150°C, which became weak at 180°C. Correspondingly, the weak peak of anatase was indexed in the case of 180°C. This observation indicates that HF did not lead to the complete conversion of Ti and Si, even at high temperature. Moreover, the series of diffraction peaks of CaF_2 (PDF = 65-0535), $NaMgAlF_6$ (PDF = 25-0841) and Ca_2AlF_7 (PDF = 83-1440) was recorded in the XRD pattern of all solid samples. The formation of these impurities was probably relative to the low solubility of metal fluorides. For instance, the solubility product constant of CaF_2 is 3.45×10^{-11} [40]. Accordingly, the incomplete conversion of Ti and Si was relative to the insoluble fluorides that was probably formed on the TBBFS surface and prevented Ti and Si from exposing to HF. This observation suggests that at high temperature, the formation of TiO_2 is predominantly improved by the HCl leaching.

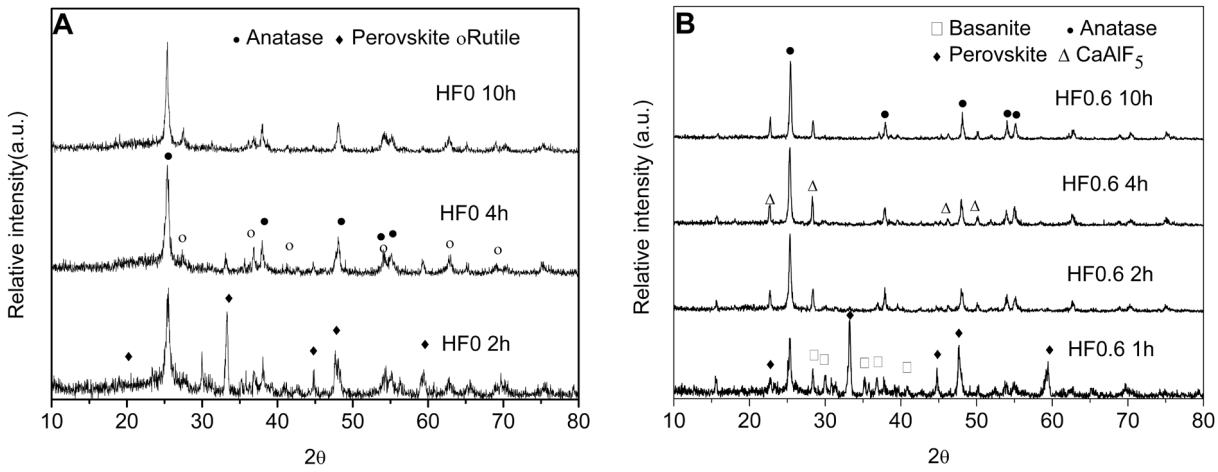

Fig. 3. XRD of TBBFS in HCl solution (A) without HF and (B) with 0.6 mol/L of HF under hydrothermal conditions.

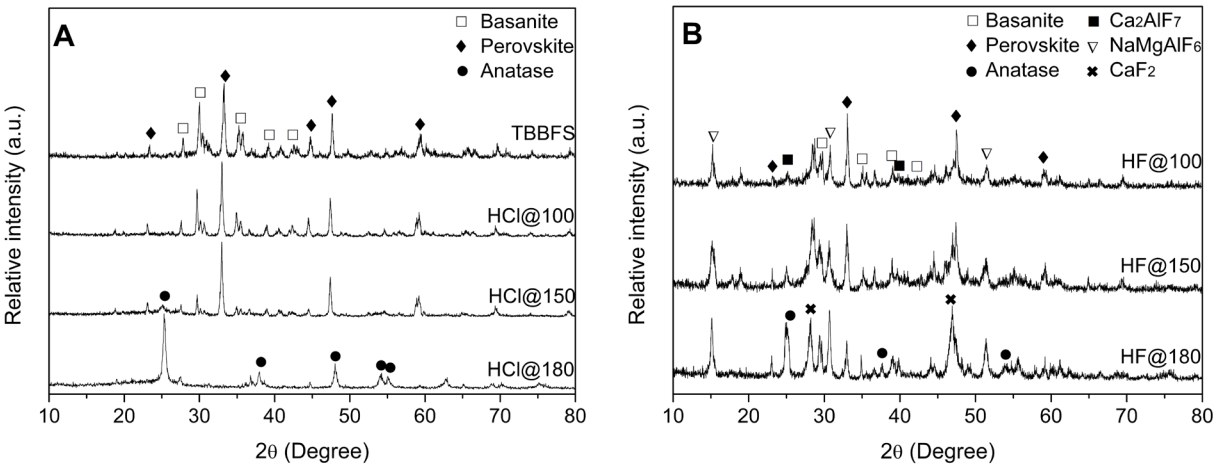

Fig. 4. XRD pattern of Ti-slag after hydrothermal treatment in HCl (A) and HF (B), compared to that of raw TBBFS.

Table 3 lists the leaching percentage of the compositions in TBBFS after hydrothermal treatment at various acidic solution. With HCl only, 3.5%–3.71% of Si and 6.36%–8.34% of Ti were leached out after hydrothermal treatment at 100°C and 150°C. This supports that Si and Ti in TBBFS kept their pristine species. In comparison, 15.7% of Si was leached out at 180°C, indicating the dissolution of basanite. Despite, the corresponding leaching percentage of Ti was reduced to 3.76%. This demonstrates that most Ti in TBBFS was in TiO_2 as the fast hydrolysis of dissolved Ti to the solid TiO_2. Moreover, the leaching percentage of Ca, Al, Fe and Mg were increased with temperature increasing, indicating the TBBFS dissolution. In the case of HF, the leaching percentage of Ti was 24.6%–37.1% at 100–150°C while was 2.98% at 180°C. The lower leaching percentage of Ti at high temperature suggests that the hydrolysis of Ti to form anatase TiO_2 was achieved in the presence of HF, consistent with the previous work [38,39]. In comparison, the leaching percentage of Si was increased with temperature increasing. Most of Si was leached out by HF at 180°C as 90.7% of Si in the HF solution after treatment. On the other hand, 25.3% of Ca and 47.6% of Al was leached out, lower than that in the case of HCl leaching. This is contributed to the precipitation of Ca and Al fluorides as the result of XRD pattern (Fig. 4B). In addition, most Mg and Fe were leached out at 180°C by HF. Thus, the tunable SiO_2/TiO_2 mass ratio was owned to the inhibition of SiO_2 conversion from basanite in TBBFS

Table 3
Leaching efficiency (%) of elements after leaching in 1 mol/L of various acid solution for 5 h

Treatment	Si[a]	Ti[b]	Ca[b]	Al[b]	Mg[b]	Fe[b]
HCl 100°C	3.50	8.34	28.7	34.6	42.9	71.8
HCl 150°C	3.71	6.36	51.7	53.7	68.3	74.2
HCl 180°C	15.7	3.76	86.0	62.0	93.7	90.1
HF 100°C	32.9	24.6	2.28	0.57	13.4	61.8
HF 150°C	72.2	37.1	3.82	1.01	16.2	60.1
HF 180°C	90.7	2.98	25.3	47.6	90.1	88.1

[a]was determined by ultraviolet spectrophotometry and [b]were determined by ICP analysis

as HF inhibited SiO_2 formation at 180°C, resulting in more exposed area of TiO_2.

3.4. Formation of SiO_2-TiO_2 composite in HCl solution

The conversion of perovskite to TiO_2 can be described by the following equations [41]:

$$CaTiO_3 + 4HCl = CaCl_2 + TiOCl_2 + 2H_2O \quad (1)$$

$$TiOCl_2 + H_2O = TiO_2 + 2HCl \quad (2)$$

As $TiOCl_2$ is unstable in the solution, the kinetics of TiO_2 formation via Ti hydrolysis was much quicker than that of Eq. (1) [42–44]. This means that the formation of TiO_2 is dependent on the dissolution of perovskite in acidic solution [Eq. (1)], which is relative to the hydrothermal temperature. Moreover, in the case of SiO_2-TiO_2 composite formation, the kinetics of SiO_2 deposition was much lower than those of Eq. (1) and Eq. (2) [45]. Accordingly, TiO_2 was formed prior to SiO_2 precipitation in the current case. Taking into account the XRD results (Fig. 3), it is obvious that the SiO_2-TiO_2 composite was formed from TBBFS leaching via dissolution of basanite and perovskite, followed by a hydrolysis of Ti and Si. At the initial stages of crystallization, the quick kinetics of TiO_2 in HCl solution led to the wrapping of TiO_2 substrate with SiO_2 that slowly deposited. Thus, the surface of TiO_2 was covered by SiO_2 at SiO_2/TiO_2 mass ratio > 1.7.

This formation process of composite was controlled by HF addition. Fig. 5 illustrates leaching amounts of Ca, Mg, Al, Ti and Si from TBBFS along with time in different acid solvents. As for Si, its leaching amount balanced at 6% of total Si amount in TBBFS after two hours without HF. This suggests most of Si formed in amorphous SiO_2 as the vanishing of basanite without new crystal Si compounds (Fig. 4B). In comparison, with HF addition, Si leaching amount increased to 20%. This was contributed to Si dissolution with the possible SiF_6^{2-} formation in HF solution. Consequently, SiO_2 deposit was inhibited by the Si dissolution and SiO_2/TiO_2 mass ratio of final product.

This hypothesis was supported by the kinetic process of Ca leaching from $CaTiO_3$. In HCl solution alone, 70% of Ca was leached out after two hours and kept increasing until 12 h (Fig. 5A). In comparison, slag in HCl and HF solvent released 70% of Ca in 4 h (Fig. 5B). For investigating the mechanism and reaction rate of perovskite leaching process, the kinetic of Ca were further fitted by various models (Table S2). The result is shown in Fig. S3. The fitting parameter is listed in Table 4. Ca leaching kinetics in HCl solvent with HF and without HF was fitted well with the pseudo-first order model as R2 value over 0.93. It is noting that all the parameter *k* in the case of HCl solvent with HF was smaller than that without HF, indicating HF could inhibit the Ca leaching from $CaTiO_3$. This is probably attributed to the CaF_2 formation on the slag surface, which kept HCl away from the $CaTiO_3$ to retard its decomposition. Besides, there is part of Ca and Al transforming to the Ca_2AlF_7 in the presence of HF (Fig. 4B). Accordingly, the slow decomposition of $CaTiO_3$ resulted in the slower generation of TiO_2 so that more TiO_2 was synthesized on the surface of SiO_2. This situation was favorable for generating SiO_2-coated TiO_2.

As for Ti, its leaching percentage was up to 5% in 1 h, and then dropped to below 1% after 4 h due to the fast hydrolysis of titanium with HCl alone. When HF was added, Ti leaching amount obviously increased, and rose until 7 h, reflecting that the addition of HF slowed the hydrolysis rate of titanium. This phenomenon could also slow TiO_2 generation to get more SiO_2-coated TiO_2. In consequence, we concluded the TiO_2 surface was exposed as SiO_2 dissolution in the HF assistance.

3.5. Performance of the photocatalyst

Fig. 6A illustrates the diffuse reflectance absorption spectra of the SiO_2-TiO_2 composite. All samples exhibited the absorbance at 200–380 nm, indicating the photoresponding of TiO_2 under UV light. Despite, the photodegradation performance of Rhodamine B (RB) was relative to the hydrothermal treatment process with various [HF]. As shown in Fig. 6B, 5% or less of RB was removed without

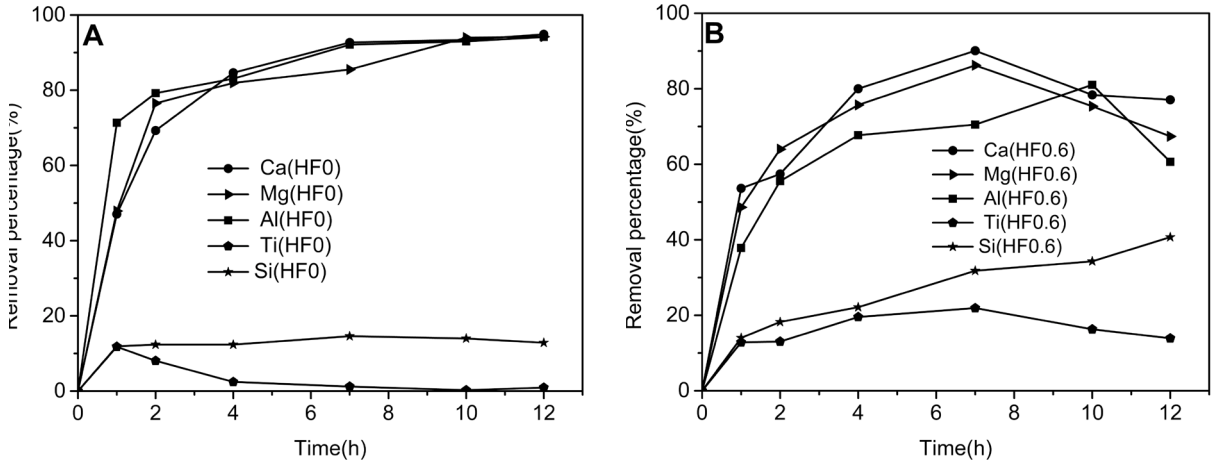

Fig. 5. Percentage of leaching elements of TBBFS in HCl solution (A) without HF and (B) with 0.6 mol/L of HF under hydrothermal conditions.

Table 4
The parameter values obtained from the Ca leaching fitting using different kinetic models

Equation Number	K (min^{-1})		q_e (mg/g)		R^2	
	Ca (0HF)	Ca (0.6HF)	Ca (0HF)	Ca (0.6HF)	Ca (0HF)	Ca (0.6HF)
Surface chemical reaction	0.0362	0.0260			0.8613	0.3898
Diffusion control	0.0460	0.0278			0.7747	0.3719
Pseudo-first order	0.6500	0.6254	93.91	84.52	0.9983	0.9361

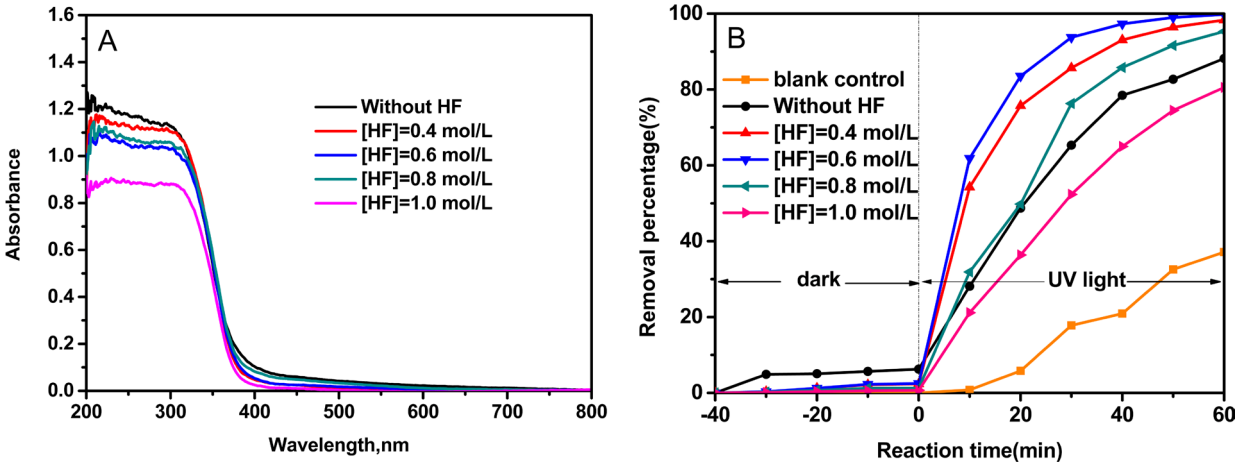

Fig. 6. The diffuse reflectance absorption spectra of the TiO_2/SiO_2 composite prepared in 1.0 mol/L HCl with various [HF]s(A) and its photocatalysis for the degradation of Rhodamine B (B).

UV light in 40 min (Dark). In comparison, the kinetics of RB removal was increased sharply under UV light. In 60 min, 35% of RB was removed without photocatalyst while more than 75% of RB was removed on the composites. This observation demonstrated that the photodegradation of RB can be achieved on the composite. Moreover, the kinetics of RB photodegradation on the composite was relative to the concentration of HF in the treatment process of TBBFS. For instance, in 50 min, the maximum removal percentage of RB was achieved on the sample HF0.4 and HF0.6.

Accordingly, this performance of RB photodegradation on the treated samples was relative to the SiO_2/TiO_2 mass ratio. As the mass ratio of SiO_2/TiO_2 was 1.1–1.2 at [HF] of 0.4–0.6 mol/L, it is proposed that the composite with SiO_2/TiO_2 ratio at 1.1–1.2 was probably a candidate for the photodegradation of contaminate in the solution. This is contributed to more surface of TiO_2 exposing for photocatalysis via the dissolution of Si in HF. On the other hand, in the case of HF0.6, the composite did not provide high SSA (Fig. S2), it is proposed that the effect of SiO_2 on the improvement of dye removal is to increase the negative change on the surface of the composite, which facilitates adsorbing organic dye on TiO_2 [46]. In addition, the low SiO_2/TiO_2 mass ratio in the composite was also obtained in the case of HF1.0. However, the fluoride formed at high [HF] probably covered the TiO_2 surface, which led to the poor photocatalysis performance. In addition, Ti, Si, and other metals were not detected in the solution after reaction, as their concentrations were lower than the detective limitation of ICP instrument. This proposed the stable composition and structure of the slag-derived photocatalyst. Therefore, the high performance of RB decomposition was contributed to the synergetic effect of TiO_2 and SiO_2 in the composite.

4. Conclusions

In this work, the hydrothermal treatment of TBBFS with HCl and HF mixture solution was performed. At 180°C, the SiO_2 coated TiO_2 composite was formed by the conversion of basanite and perovskite in TBBFS. The XRD characterization of the product showed the anatase phase with amorphous SiO_2 was formed in the composite, Moreover, the photocatalysis was also impacted by the mass ratio of SiO_2 to TiO_2. Accordingly, the SiO_2/TiO_2 mass ratio was reduced to 1.1–1.2 on the product by decreasing the concentration of HF in mixture solution, which removed 95% or more Rhodamine B under UV light irradiation. Our results proposed that the hydrothermal treatment of TBBFS in the mixture solution with HCl and HF was a promising way to provide a photocatalyst candidate from TBBFS for the effective degradation of organic contaminate in the solution.

Acknowledgements

This project was financially supported by National Nature Science Foundation of China Nos. 21207086, 51174132, 20907029, and 20877053, National Natural Science Foundation of China No.11025526, Science and Technology

Commission of Shanghai Municipality No. 13230500600, Program for Innovative Research Team in University No.IRT13078 and Shanghai Leading Academic Discipline Project No. S30109.

References

[1] Y.S. Lu, X.X. Yang, L. Xu, Z. Wang, Y.F. Xu, G.R. Qian, Sulfate radicals from Fe^{3+}/persulfate system for Rhodamine B degradation, Desal. Water Treat., 57 (2016) 29411–29420.
[2] L.X. Qin, Q. Luo, K.J. Liang, S.Z. Kang, G.D. Li, X.Q. Li, Highly efficient decomposition of rhodamine B in wastewater with graphene/silver-based nanocomposite catalyst: process optimization and kinetics, Desal. Water Treat., 84 (2017) 40–47.
[3] U.B. Ogutveren, M. Ogutveren, Green synthesis of iron nano-materials by plants and their use in removal of pollutants from wastewaters - a review, Desal. Water Treat., 78 (2017) 141–154.
[4] Y.S. Lu, Z. Wang, Y.F. Xu, Q. Liu, G.R. Qian, Fe-2(MoO4)(3) as a novel heterogeneous catalyst to activate persulfate for Rhodamine B degradation, Desal. Water Treat., 57 (2016) 7898–7909.
[5] X.B. Chen, S.S. Mao, Titanium dioxide nanomaterials: synthesis, properties, modifications, and applications, Chem. Rev., 107 (2007) 2891–2959.
[6] A. Haarstrick, O.M. Kut, E. Heinzle, TiO_2-assisted degradation of environmentally relevant organic compounds in wastewater using a novel fluidized bed photoreactor, Environ. Sci. Technol., 30 (1996) 8.
[7] D. Zhao, C.C. Chen, Y.F. Wang, W.H. Ma, J.C. Zhao, T. Rajh, L. Zang, Enhanced photocatalytic degradation of dye pollutants under visible irradiation on Al(III)-modified TiO_2-structure, interaction, and interfacial electron transfer, Environ. Sci. Technol., 38 (2008) 308–314.
[8] H. Tada, Y. Kubo, M. Akazawa, S. Ito, Promoting effect of SiOx monolayer coverage of TiO_2 on the photoinduced oxidation of cationic surfactants, Langmuir, 14 (1998) 2936–2939.
[9] H. Tada, M. Yamamoto, S. Ito, Promoting effect of MgOx submonolayer coverage of TiO_2 on the photoinduced oxidation of anionic surfactants, Langmuir, 15 (1999) 3699–3702.
[10] Y.M. Xu, C.H. Langford, Photoactivity of titanium dioxide supported on MCM-41, zeolite X, and zeolite Y, J. Phys. Chem. B, 101 (1997) 3115–3121.
[11] W. Wei, S. Mo, Photocatalytic activity of titania-containing mesoporous SBA-15 silica, Microporous Mesoporous Mater., 96 (2006) 255–261.
[12] W. Patrick, S. Dietmar, Photodegradation of rhodamine B in aqueous solution via SiO_2@TiO_2 nano-spheres, J. Photochem. Photobiol. A, 185 (2007) 19–25.
[13] J.C. Zhao, T.X. Wu, K.Q. Wu, K. Oikawa, H. Hidaka, N. Ssrpone, Photoassisted degradation of dye pollutants. 3. Degradation of the cationic dye rhodamine B in aqueous anionic surfactant/TiO_2 dispersions under visible light irradiation: evidence for the need of substrate adsorption on TiO_2 particles, Environ. Sci. Technol., 32 (1998) 2394–2400.
[14] H. Ijadpanah-Saravi, M. Zolfaghari, A. Khodadadi, P. Drogui, Synthesis, characterization, and photocatalytic activity of TiO_2-SiO_2 nanocomposites, Desal. Water Treat., 57 (2016) 14647–14655.
[15] J. Angkhana, P. Nuchanaporn, K. Nudthakarn, S. Ron, Nanocomposite TiO_2–SiO_2 gel for UV absorption, Chem. Eng. J., 181–182 (2012) 45–55.
[16] Z. Liu, F.T. Chen, P.F. Fang, S.J. Wang, Y.P. Gao, F. Zheng, Y. Liu, Y.Q. Dai, Study of adsorption-assisted photocatalytic oxidation of benzene with TiO_2/SiO_2 nanocomposites, Appl. Catal. A- Gen., 451 (2013) 120–126.
[17] W.Y. Dong, C.W. Lee, X.C. Lu, Y.J. Sun, W.M. Hua, G.S. Zhuang, S.C. Zhang, J.M. Chen, H.Q. Hou, D.Y. Zhao, Synchronous role of coupled adsorption and photocatalytic oxidation on ordered mesoporous anatase TiO_2–SiO_2 nanocomposites generating excellent degradation activity of RhB dye, Appl. Catal. B: Environ., 95 (2010) 197–207.
[18] A. Haghighatzadeh, B. Mazinani, M.S. Asl, L. Bakhtiari, TiO_2 (rutile and anatase) deposited on ordered mesoporous SiO_2: effect of pore size on photocatalytic activity, Desal. Water Treat., 80 (2017) 156–163.
[19] R. Mohammadi, Influence of preparation method on the physicochemical properties and catalytic activity of SiO_2-TiO_2 mixed oxides, Desal. Water Treat., 57 (2016) 22370–22377.
[20] M. Homayoonfal, M.R. Mehrnia, Y.M. Mojtahedi, A.F. Ismail, Effect of metal and metal oxide nanoparticle impregnation route on structure and liquid filtration performance of polymeric nanocomposite membranes: a comprehensive review, Desal. Water Treat., 51 (2013) 3295–3316.
[21] J.H. Jhaveri, Z.V.P. Murthy, Nanocomposite membranes, Desal. Water Treat., 57 (2016) 26803–26819.
[22] X.F. Lei, X.X. Xue, Preparation and characterization of perovskite-type Titania-bearing blast furnace slag photocatalyst, Mater. Sci. Semicond. Process., 11 (2008) 117–121.
[23] X.F. Lei, X.X. Xue, H. Yang, Preparation of UV-visible light responsive photocatalyst from titania-bearing blast furnace slag modified with $(NH_4)_2SO_4$, T. Nonferr. Metal. Soc., 22 (2012) 1771–1777.
[24] K.M. Parida, N. Sahu, N.R. Biswal, B. Naik, A.C. Pradhan, Preparation, characterization, and photocatalytic activity of sulfate-modified titania for degradation of methyl orange under visible light, J. Colloid Interface Sci., 318 (2008) 231–237.
[25] H. Liu, T. Xia, H.K. Shon, S. Vigneswaran, Preparation of titania-containing photocatalysts from metallurgical slag waste and photodegradation of 2,4-dichlorophenol, J. Ind. Eng. Chem., 17 (2011) 461–467.
[26] L. Zhang, L.N. Zhang, M.Y. Wang, G.Q. Li, Z.T. Sui, Recovery of titanium compounds from molten Ti-bearing blast furnace slag under the dynamic oxidation condition, Miner. Eng., 20 (2007) 684–693.
[27] L. Zhang, L.N. Zhang, M.Y. Wang, T.P. Lou, Z.T. Sui, J.S. Jang, Effect of perovskite phase precipitation on viscosity of Ti-bearing blast furnace slag under the dynamic oxidation condition, J. Non-Cryst. Solids, 352 (2006) 123–129.
[28] X.F. Lei, X.X. Xue, Preparation, characterization and photocatalytic activity of sulfuric acid-modified titanium-bearing blast furnace slag, T. Nonferr. Metal. Soc., 20 (2010) 2294–2298.
[29] X.F. Lei, X.X. Xue, H. Yang, Effect of preparation method on photocatalytic activity of titanium-bearing blast furnace slag, Adv. Mater. Res., 690–693 (2013) 1081–1085.
[30] M. Balakrishnan, V.S. Batra, J.S.J. Hargreaves, I.D. Pulford, Waste materials – catalytic opportunities: an overview of the application of large scale waste materials as resources for catalytic applications, Green Chem., 13 (2011) 16–24.
[31] T.Y. Xue, L. Wang, T. Qi, J.L. Chu, J.K. Qu, C.H. Liu, Decomposition kinetics of titanium slag in sodium hydroxide system, Hydrometallurgy, 95 (2009) 22–27.
[32] K. Yasutaka, O. Tetsutaro, M. Kohsuke, K. Iwao, Y. Hiromi, Synthesis of zeolite from steel slag and its application as a support of nano-sized TiO_2 photocatalyst, J. Mater. Sci., 43 (2007) 2407–2410.
[33] Z.H. Zhang, X.N. He, Q. Jin, T.F. Lv, Determination of Si(IV) in ZSM-5 zeolites by spectrophotometry, J. Beijing Inst. Petro-chem. Technol., 18 (2010) 43–46.
[34] S.G. Yang, C. Sun, X.Y. Li, Z.Q. Gong, X. Quan, Enhanced photocatalytic activity for titanium dioxide by co-modifying with silica and fluorine, J. Hazard. Mater., 175 (2010) 258–266.
[35] S. Yuan, L.Y. Shi, K. Mori, H. Yamashita, Preparation of highly dispersed TiO_2 in hydrophobic mesopores by simultaneous grafting and fluorinating, Micropor. Mesopor. Mat., 117 (2009) 356–361.
[36] Y. Li, L.L. Liu, M. Guo, M. Zhang, Synthesis of TiO_2 visible light catalysts with controllable crystalline phase and morphology from Ti-bearing electric arc furnace molten slag, J. Environ. Sci. China, 47 (2016) 14–22.
[37] M.S. Vohra, K. Tanaka, Photocatalytic degradation of aqueous pollutants using silica-modified TiO_2, Water Res., 37 (2003) 3992–3996.

[38] W.Q. Fang, J.Z. Zhou, J. Liu, Z.G. Chen, C. Yang, C.H. Sun, G.R. Qian, J. Zou, S.Z. Qiao, H.G. Yang, Hierarchical structures of single-crystalline anatase TiO_2 nanosheets dominated by {001} facets, Chemistry, 17 (2011) 1423–1427.
[39] C.Z. Wen, J.Z. Zhou, H.B. Jiang, Q.H. Hu, S.Z. Qiao, H.G. Yang, Synthesis of micro-sized titanium dioxide nanosheets wholly exposed with high-energy {001} and {100} facets, Chemical Commun., 47 (2011) 4400–4402.
[40] W.M. Haynes, Handbook of Chemistry and Physics, in: Solubility Product Constants CRC Press, Florida, 2011, pp. 1344.
[41] L.G. Gerasimova, M.V. Maslova, E.S. Shchukina, Obtaining of titanium-containing products via the hydrochloric acid processing of grothite and perovskite, Theor. Found. Chem. Eng., 45 (2011) 511–516.
[42] E. Olanipekun, A kinetic study of the leaching of a Nigerian ilmenite ore by hydrochloric acid, Hydrometallurgy, 53 (1999) 1–10.
[43] N.Y. Mostafa, M.H.H. Mahmoud, Z.K. Heiba, Hydrolysis of $TiOCl_2$ leached and purified from low-grade ilmenite mineral, Hydrometallurgy, 139 (2013) 88–94.
[44] M. Madekufamba, L.N. Trevani, P.R. Tremaine, Standard enthalpy of formation of aqueous titanyl chloride, $TiOCl_2$(aq), at T = 298.15K, J. Chem. Thermodyn., 38 (2006) 1563–1567.
[45] Y.N. Kim, G.N. Shao, S.J. Jeon, S.M. Imran, P.B. Sarawade, H.T. Kim, Sol–gel synthesis of sodium silicate and titanium oxychloride based TiO_2–SiO_2 aerogels and their photocatalytic property under UV irradiation, Chem. Eng. J., 231 (2013) 502–511.
[46] C. Minero, F. Catozzo, E. Pelizzett, Role of adsorption in photocatalyzed reactions of organic molecules in aqueous titania suspensions, Langmuir, 8 (1992) 481–486.

Supplemental information

Table S1
The composition of the TBBFS after hydrothermal treatment at 180°C in 1 mol/L HCl solution with various HF addition. (%, w/w)

Treatment	Si[a]	Ti[a]	Ca[a]	Al[a]	Mg[a]	Fe[a]
0.4HF	9.4	10.3	1.6	1.3	0.3	0
0.6HF	8.2	9.1	2.1	2.1	1.1	0
0.8HF	7.8	2.9	5.5	2.3	0.9	0
1.0HF	6.7	4.9	9.1	2.8	1.2	0

[a]was determined by XRF (XRF-1800)

Table S2
Different kinetic models used to study the Ca leaching from TFFBS with and without HF

Kinetic model	Equation	
Surface chemical reaction	$1-(1-)^{1/3}=k_1t$	(3)
Diffusion control	$1-3(1-)^{2/3}+2(1-)=k_2t$	(4)
Pseudo-first order kinetic model		(5)

where k_1 to k_4 (min^{-1}) are rate constant for corresponding kinetic models, Q_{e1} and Q_{e2} (%) are equilibrium leaching percentage of first and secondary order kinetics respectively, t (min) is time, Q_t is the total leaching percentage at time t. Eq. (3) and Eq. (4) called shrinking core model (SCM) are based on surface chemical reactions and diffusion severally in a liquid/solid reaction system. The pseudo-first order kinetic model which was used for solid–liquid heterogeneous systems commonly gave expression to the law of Ca leaching from TFFBS over time.

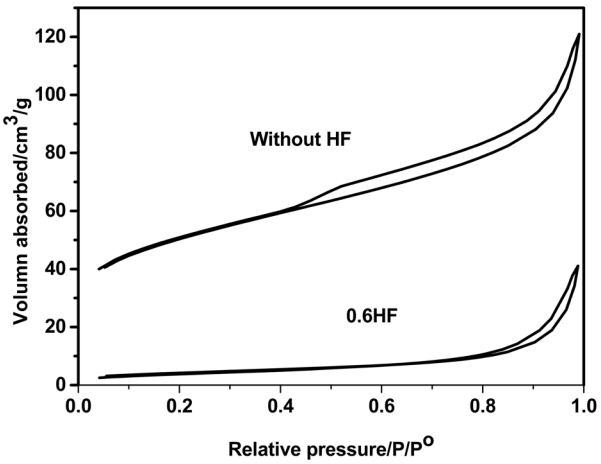

Fig. S1. N_2 adsorption-desorption curve of the sample after hydrothermal treatment without HF and with 0.6 mol/L HF.

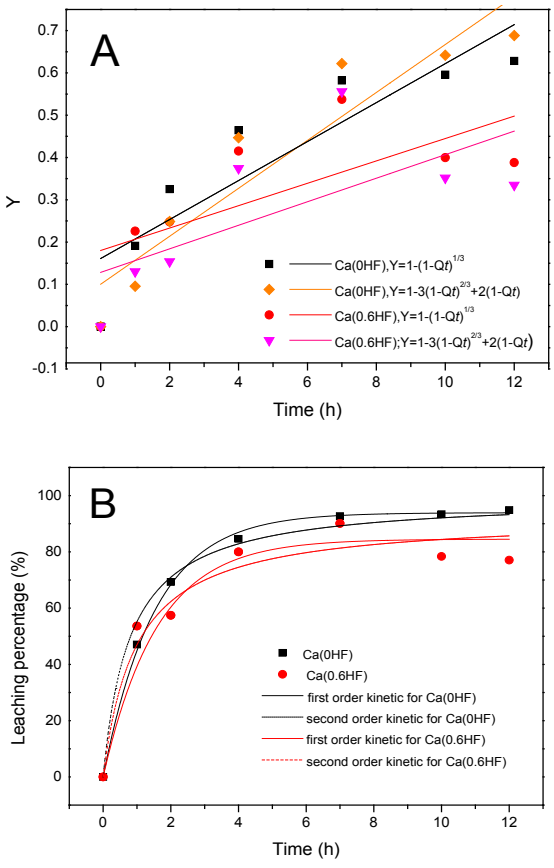

Fig. S2. The kinetic fitting plots of Ca leaching with and without HF by (A) Eq. (3) and Eq. (4); (B) by Eq. (5) and Eq. (6).